Journal of Innovative Optical Health Sciences
Vol. 8, No. 1 (2015) 1540002 (9 pages)

DOI: 10.1142/S1793545815400027

World Scientific
www.worldscientific.com

Effects of wavelength, beam type and size on cerebral low-level laser therapy by a Monte Carlo study on visible Chinese human

Ting Li*, Yue Zhao, Yunlong Sun and Kai Li
School of Microelectronics & Solid-State Electronics, Biomedical Engineering
University of Electronic Science & Technology of China
Chengdu 610054, P. R. China
**liting@uestc.edu.cn*

Received 30 October 2013
Accepted 26 December 2013
Published 20 February 2014

Low-level laser therapy (LLLT) has been clinically utilized for many indications in medicine requiring protection from cell/tissue death, stimulation of healing and repair of injuries, pain reduction, swelling and inflammation. Presently, the use of LLLT to treat stroke, traumatic brain injury and cognitive dysfunction are attracting growing interest. Near-infrared light is capable of penetrating into the cerebral cortex, allowing noninvasive treatments to be carried out with few treatment-related adverse events. Optimization of LLLT treatment effect is a crucial issue of this field; however, only a few experimental tests on mice for wavelength selection have been reported. We addressed this issue by low-cost, straightforward and quantitative comparisons on light dosage distribution within visible Chinese human head by Monte Carlo modeling of near-infrared light propagation. Optimized selection in wavelength, beam type and size were given based on comparisons among frequently used setups (i.e., wavelengths: 660, 810 and 980 nm; beam type: Gaussian and flat beam; beam diameter: 2, 4 and 6 cm). This study provided an efficient way for guiding the optimization of LLLT setup and selection on wavelength, beam type and size for clinical brain LLLT.

Keywords: Low level laser therapy; visible Chinese human; Monte Carlo simulation; beam; wavelength.

1. Introduction

Moderate and severe traumatic brain injury (TBI), accidental or inflicted, is a socio-economic and major health problem throughout the world.[1] The world health organization (WHO) has projected that the road traffic accidents, a major cause of TBI, will rank the third cause for the global burden of disablement and disease, behind merely the head ischemic disease and unipolar depression.[1–4] This has led the WHO to set a priority for prevention of head injuries, however, the occurrence rate of head injuries keep increasing throughout the world.

Efforts to improve treatment and outcome must therefore be the emergent priority for clinicians and researchers.[1] Of note, TBI pathophysiology is complicated and still poorly understood. Quickly following the primary impact, activation of several different pathways begins and accordingly results in secondary brain injury, including oxidative stress, ionic imbalance, inflammation, increased vascular permeability, mitochondrial dysfunction, etc.[5,6] The combination of cellular and physiologic disturbances causes increased neuronal cell death, enlarging the infarct area and neurological impairment (e.g., motor and cognition). Presently, there is no effectively approved drugs blocking the secondary injury progression; the current management of TBI mainly aims at curing brain edema, combating hypoxia and shock.[4] Unfortunately, most of the performed trails in recent years have failed to prove any significant improvement.[7]

Low-level laser (or light) therapy (or treatment) LLLT has been clinically applied for many medication indications requiring the following processes, including protection from cell and tissue death, reduction of pain, repair of injuries and stimulation of healing, swelling and inflammation.[3,8] One field which is attracting more and more interest is the use of LLLT in treatment of TBI, stroke, neurodegenerative diseases and spinal cord injuries.[6] The well-known significant drawback of any effective drug-based treatments for most of the above diseases has motivated researchers to explore the proper way to use light as an effective approach to mitigating or curing those grouped serious diseases. The principle that near-infrared light can penetrate into the brain/spinal cord allows noninvasive treatment to be operated on patients with a minimum likelihood of treatment-related adverse events. In the past few years, nevertheless, people generally thought that the central nervous system could not repair itself, but recent reports showed that neuronal stem cells had questioned this dogma.[5] LLLT was highlighted to have beneficial effects in a series of acute treatment on traumatic brain damage and stroke by improving mitochondrial function, inhabiting neuronal apoptosis, reducing the excitotoxicity consequent upon glutamate release and up regulating several protective factors.[3,9]

LLLT, existing as a potential therapeutic tool for serious medical issues causing significant morbidity and mortality to mankind, remains controversial.[3] This likely contributed to two main reasons. One is the complexity of optimized selection among a large number of illumination parameters, including light wavelength, beam size, beam type, fluence, power density, pulse structure and treatment timing.[3,10] This issue has led to a number of reported negative studies as well as lots of positive ones.[3,11] Particularly, some dose treatment trails has observed that low-level light has a much better effect than higher-level light.[3] Qualitatively optimizing the illumination parameters would improve the LLLT treatment outcome. Recently, researchers performed a lot of experiments on animal model, such as dog, rat and rabbit, to get the rough range in choosing some specified illumination parameters. Using experiments to optimize the illumination suffered several disadvantages, such as high cost and time-consuming, low reliability and precision due to the difficulty in distinguishing the effect of illumination parameter and physiological conditions of the animals and unreality to use living human model directly. Apparently, a new method overcoming the above disadvantages is imperative for quantitatively optimizing the illumination parameters for both research and clinics on LLLT.

Near-infrared light propagation in brain is an important issue for both monitoring and treatment uses of near-infrared light.[12] For near-infrared therapy, there are many research challenges including its mechanism underlying the cure effects and the complexity of rationally setting a large number of illumination parameters.[3,13] The calculation of fluence distribution in human head benefits in understanding the mechanism and optimization of near-infrared therapy.[12] Such light fluence distribution within tissue is impractical to be directly measured by experiments. Diffusion approximation can provide the fluence distribution in simple-geometry tissue, such as infinite/semi-infinite tissue, but cannot give an analytical solution in arbitrary-geometry tissue. Monte Carlo simulation has been widely used to simulate light propagation in tissues and gone through several improvements since introduced to the field of laser–tissue interactions. It has provided a reliable, precise and flexible calculation of light propagation in realistic-structured biological tissues, such as multi-layered biological tissue.[14] Recently, researchers have developed the Monte Carlo simulation model and relative software for three-dimensional (3D) optical properties spatial-resolved tissues, such as the complex-structured human head.[15] Meanwhile, there are

several standard visible human dataset released to the world providing the anatomic structure of our human for medicine and production usages,[16] which provided high realistic head model for Monte Carlo simulation of fluence distribution for LLLT. Among these visible humans, visible Chinese human (VCH) achieved highest spatial resolution and finest segmentation of different type of tissues in the whole body, and is considered as the most precise human structure model.[17–20]

This paper aimed to obtain quantitative optimization of LLLT by calculating light fluence distribution in human head based on the combination between Monte Carlo simulation and VCH. In order to simulate fluence distribution in the VCH head, the simulation method applicable for 3D voxelized media was required since the VCH head was a voxelized model. Actually, a software program targeted for Monte Carlo simulation of light propagation in voxelized media (MCVM), which is applicable for the VCH, has been developed and fully tested. By using MCVM and VCH, our interest here was to evaluate the light fluence distribution in the VCH head with concern on the preference in choosing wavelengths, beam type and beam size for cerebral LLLT. Optimized selection in wavelength, beam type and size were given based on comparisons among frequently used setups (i.e., wavelengths: 660 nm, 810 nm, 980 nm[21,22]; beam type: Gaussian and flat (Top-hat) beam[23]; beam diameter: 2, 4 and 6 cm[23]). We believed that, to our best knowledge, this was the first demonstration using Monte Carlo-VCH model-based fluence simulation to solve quantitative optimization for choosing the important illumination.

2. Methods

2.1. *VCH head*

Details on developing the VCH phantom, including the image acquisition and segmentation, have been described in Refs. 19–21. Briefly, the VCH specimen, a male adult, was frozen in the standing posture, and horizontally sectioned at 0.02-cm interval. Digital color photographs of the top surface after each sectioning were obtained with the resolution of 0.01 cm per pixel, which is higher than computed tomography (CT) or Magnetic Resonance Imaging (MRI) data (such as Zubal model). The segmentation of VCH, unlike CT or MRI data, was performed based on these color photographs, with little dependence on pixel gray values. Under the direction of experienced anatomists, distinct tissues in each slice were visibly distinguished, manually segmented and labeled with a specified identification number. The advantages, including high resolution and precise segmentation, make the VCH most realistically represent human anatomical structures. Particularly, the upstanding posture of VCH, instead of lying down in MRI or CT, was able to present more realistic geometry of brain surface for light propagation prediction.

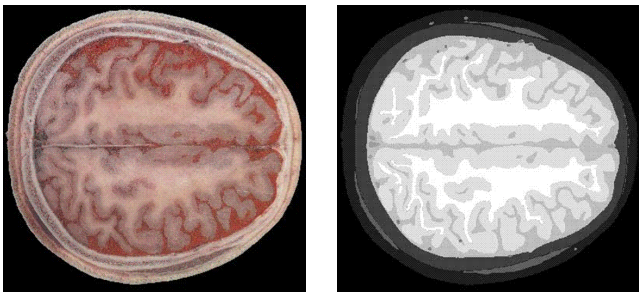

(a) (b)

Fig. 1. VCH head model. (a) Digital color photograph of one slice in the VCH head dataset; (b) Segmentation of the slice in (a).

The color photographs and the segmented datasets of the VCH forehead were extracted for use. The head model has been segmented into at least eight types of tissue (see Fig. 1 for one slice), including scalp, skull, CSF, muscle, visible artery/vein blood vessels, gray and white matter. For the segmented dataset, every four consecutive pixels along both anterior-posterior and left-right directions in every two consecutive slices were chosen to form voxels each of $0.04 \times 0.04 \times 0.04\,\text{cm}^3$. This was just the voxel size in our simulation on common personal computer to balance the computation time and precision. We finally obtained a 3D matrix of $450 \times 400 \times 150$ voxels containing the indices for different head tissue types. The indices were used to assign tissue-specific optical properties for each voxel. The optical properties of these tissues at 660, 810 and 980 nm were listed in Table 1.[25–28] In particular, these optical properties were equal to or close to the related previous studies.[12,24,30]

2.2. *MCVM method*

Monte Carlo simulation was used to predict light fluence distribution in the VCH forehead. The

Monte Carlo software used here was targeted for 3D voxelized media (MCVM), the algorithm of which has been described in detail in Ref. 15. Briefly, photon propagation in the head was determined by scattering coefficient, tiny absorption coefficient, phase function and reflections/refractions in the 3D arbitrary surface of the tissue and complex interfaces between different types of tissue. Notably, the scattering length was segmented to a series of substeps, each of which should be smaller than voxel side-length. Once the photon traveled through a substep, it was checked whether the photon had crossed a boundary between different tissues, to track each reaction rigorously and precisely. Particularly, when a photon crossed a refractive-index mismatched boundary, reflection and refraction would be considered, including the surface of the head and interfaces between different tissue types. Of note, if the photon had indeed crossed a boundary in a substep, the substep would be renewed as the initial section of the substep to the first-met-boundary. By this way, each actual substep was relative to a single voxel, and of cause relative to a single absorption coefficient. Consequently, the absorption related with such substep was recorded precisely to the local voxel by pseudo continuous absorption weighting. Additionally, the scattering length would be corrected when a photon crossed the boundary of voxels with different scattering coefficients. MCVM has been validated well with both theoretical data and experimental data.[15,24,30]

The simulation setup parameters in the input file and the head structure file were prepared before running MCVM simulations. Basically, we setup the input/output file name, the illumination position and directions, number of photons indicating the illumination power, the beam type and beam size, as well as the optical properties of each type of tissue included in the whole head. Besides, we incorporated the segmentation files to a 3D matrix respective to the VCH head by indexing each type of tissue. After writing the tissue structure matrix to a specified format defined by MCVM software, we were able to run the software MCVM, and input the setup file name. MCVM computed the light propagation and kept reporting the remaining time. Finally, MCVM outputted the 3D absorption distribution and the escaped photon information out of the tissue.

2.3. *Monte Carlo simulation*

We set 3 (wavelengths: 660, 810 and 980 nm) × 2 (beam types: Gaussian beam and flat beam) × 3 (beam diameter: 2, 4 and 6 cm), totally 18 simulations. 10^7 photons were launched for each simulation. Each simulation was repeated for 10 times and the output was averaged for data analysis to increase the signal-to-noise ratio. The setup for wavelength was carried out by inputting the wavelength-dependent optical properties for all types of tissue in the VCH head (see Table 1). Beam type and size were set directly in the input parameters in the input file of MCVM simulation. For comparison among the effects of wavelengths, beam types and beam sizes, we kept the beam center position in the center of forehead 1 cm above the eyebrow, and kept the inject direction of the beam at the normal direction of the forehead. After all simulations, we calculated the fluence distribution by dividing the output light absorption distribution by the absorption coefficient distribution in the

Table 1. Optical properties of head tissues for 660-nm, 810-nm and 980-nm light.[25–28] The units of both absorption coefficient (u_a) and scattering coefficient (u_s) are cm^{-1}. Those tissue types having no anisotropic factor (g) value in the table denoted that their g was set as 0.9 in default.

	660			810			980		
Wavelength (nm)	u_a	u_s	g	u_a	u_s	g	u_a	u_s	g
Scalp	0.34	25.8	–	0.195	19.2	–	0.45	14.0	–
Skull	0.30	24.3	–	0.165	15.6	–	0.36	11.5	–
CSF	0.04	3.5	–	0.05	2.4	–	4.5	1	–
Gray matter	0.22	880	0.85	0.3	700	0.892	0.5	550	–
White matter	0.82	4000	0.84	1	3500	0.862	1.4	3000	0.88
Muscle	0.87	8.61	–	0.27	6.87	–	0.55	5.65	–
Arterial blood	1.30	611	0.995	2.33	500	0.993	2.90	374	0.992
Venous blood	4.87	250	0.995	2.38	522	0.993	1.62	515	0.992

tissue. We compared and analyzed the fluence distributions to address the optimization issue on selection of wavelength, beam type and beam size for brain LLLT.

3. Results

3.1. *Wavelength and beam type*

The fluence distribution in the VCH brain was shown in the slice placing the beam center. The effect of choosing different beam type and wavelengths on light fluence distribution was shown in Fig. 2. The iso-F contours were shown for 10^{-5}, 10^{-4}, 10^{-3} and 10^{-2} W/cm^2. Apparently, the wavelength selection took stronger effect than beam type in near-infrared LLLT fluence (dosage) distribution.

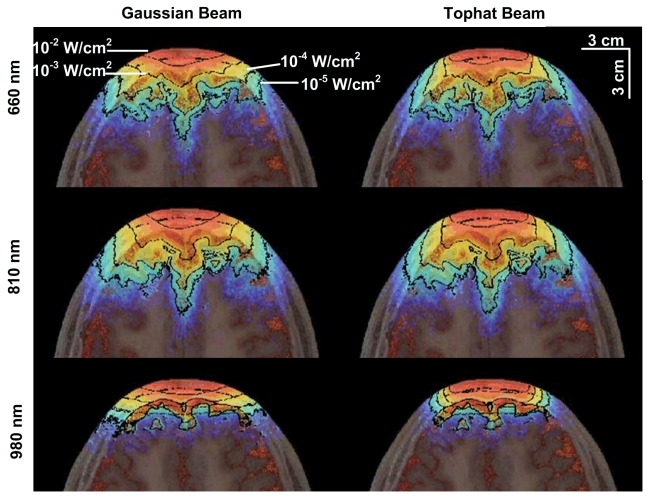

Fig. 2. The LLLT fluence distribution respective to Gaussian and Tophat (flat) beams at different wavelengths.

810 nm was shown to be more capable than 660 and 980 nm in penetrating deeper and wider into the brain tissue. The iso-F contours at 10^{-3} W/cm^2 for 660 and 810 nm has already touched the superficial layer of gray matter, while that for 980 nm has not. We observed that the iso-F contours at 10^{-4} W/cm^2 for 810 nm penetrated similarly deeper as the ones at 10^{-5} W/cm^2 for 660 nm. Quantitatively, the iso-F contour at 10^{-5} W/cm^2 for 810 nm penetrated 0.5 cm deeper than for 660 nm. The 660 nm light penetrated the modest depth into the brain tissue and 980 nm merely penetrated into the brain tissue (gray matter or white matter). It seems that 980 nm only took the treatment effect on the superficial tissue of the VCH head, including the skin and skull layers. Such strong effect of wavelength was also identified by statistics (see Tables 2 and 3). The light-penetrated voxels within brain tissue for 810 nm were 23% more than those for 660 nm and were 3.5X more than those for 980 nm (see Table 2). The sum fluence within brain tissue for 810 nm was <1X higher than that for 660 nm and was >30X higher than that for 980 nm (see Table 3).

On the other hand, beam type took weaker effect than wavelength on LLLT dosage distribution in the brain. The only significant difference between Gaussian and Top-hat beams happened to 10^{-2} W/cm^2 iso-F contours. Gaussian beam formed a more focused fluence distribution in this contours than Top-hat beam. When we compared the number (see Table 2) and sum fluence (see Table 3) of penetrated voxels within brain tissue, we found Gaussian beam acted a little bit weaker light penetration than

Table 2. Mean numbers of light penetrated voxels within brain tissue. Std < 0.01%Mean.

Wavelength (nm)	660		810		980	
	Gaussian	Top-hat	Gaussian	Top-hat	Gaussian	Top-hat
Gray matter	994,849	1003,640	1220,421	1224,844	268,118	262,267
White matter	89,371	91,295	138,312	139,132	8,981	8,703

Table 3. Accumulated fluence of light-penetrated voxels within brain tissue. Std < 0.01%Mean.

Wavelength (nm)	660		810		980	
	Gaussian	Top-hat	Gaussian	Top-hat	Gaussian	Top-hat
Gray matter	3.81e-2	4.06e-2	4.78e-2	4.99e-2	1.20e-3	1.48e-3
White matter	9.26e-5	9.98e-5	1.49e-4	1.55e-4	2.26e-7	2.58e-7

Top-hat beam. Top-hat beam penetrated $<2\%$ more voxels than Gaussian beam in brain tissues for both 810 and 660 nm. Gaussian beam penetrated $\sim 2\%$ more voxels than Top-hat beam within brain tissue at 980 nm, which was ignorable because 980-nm light showed ignorable penetration into brain tissue and the numbers of penetrated voxels within brain tissue were quite less than other wavelengths (see Table 2). Also, the Top-hat beam penetrated $\sim 4-20\%$ higher accumulated fluence than Gaussian beam for all studied wavelengths (see Table 3).

3.2. *Beam size and beam type*

The fluence distribution respective to different beam size and type in the VCH head is shown in Fig. 3. Diameter is represented with the notation "d" in Fig. 3 and Tables 4 and 5. It was obvious that the fluence distributed into a wider region followed with the beam diameter increment, especially for $10^{-2}\,\mathrm{W/cm^2}$, $10^{-3}\,\mathrm{W/cm^2}$ and $10^{-4}\,\mathrm{W/cm^2}$ iso-F contours. Interestingly, followed with beam size increment, the effect of the folding cerebral cortex geometry on the fluence distribution decreased significantly. The additional penetration depth of fluence at center normal direction decreased with beam size. Such effect of beam size on LLLT dosage distribution kept consistent, no matter what kind of beam being used (e.g., Gaussian beam, Top-hat beam). The finding that light penetration within brain tissue was increased with beam diameter was also evident by light-penetrated brain tissue voxel number statistics (see Table 4). The penetrated voxels within brain tissue for $d = 4\,\mathrm{cm}$ and $d = 6\,\mathrm{cm}$ beams were around 4.5% and 5.5% more than for $d = 2\,\mathrm{cm}$, respectively. Table 5 also showed that the accumulated fluence within brain tissue voxels was increased by beam diameter for both beam types. The sum fluence within brain tissue for $d = 4\,\mathrm{cm}$ and for $d = 6\,\mathrm{cm}$ were 29% and 51% higher than for $d = 2\,\mathrm{cm}$.

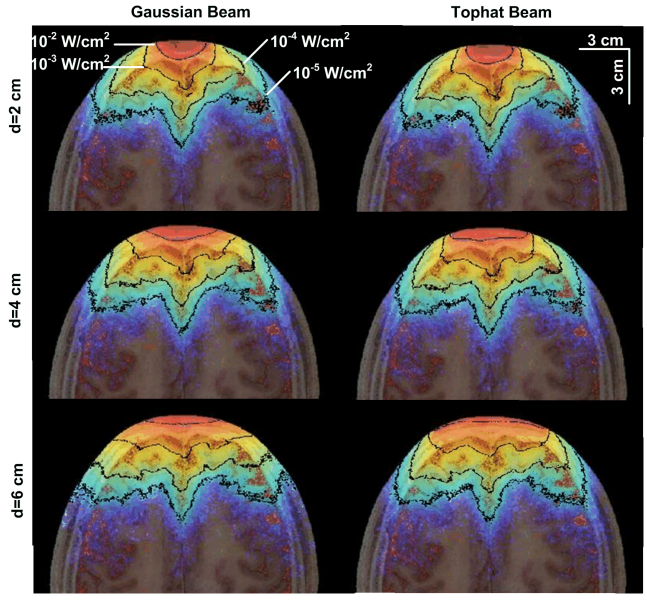

Fig. 3. The LLLT fluence distribution respective to Gaussian and Tophat (flat) beams at different diameter.

There was not much difference between beam types as beam size increased in whole fluence distribution (see Fig. 3), while the voxel numbers and accumulated fluence for light penetrated brain tissue showed obvious difference between beam types (see Tables 4 and 5). The $> 10^{-3}\,\mathrm{W/cm^2}$ fluence distribution of Gaussian beam kept a significant focusing characteristic in smaller beam diameter range (e.g., 2 and 4 cm). This focusing characteristic of fluence distribution from Gaussian beam reduced a lot for $d = 6\,\mathrm{cm}$. The preference of Top-hat beam was also quantitatively supported by Tables 4 and 5. The Top-hat beam acted $\sim 1\%$ stronger penetration than Gaussian beam for all diameter setups by light-penetrated brain tissue voxels (see Table 4). Table 5 also showed that Top-hat beam provided $\sim 4-16\%$ higher accumulated fluence within brain tissue than for Gaussian beam for both $d = 2\,\mathrm{cm}$ and $d = 4\,\mathrm{cm}$. While for $d = 6\,\mathrm{cm}$, Gaussian beam showed $\sim 6-13\%$ higher accumulated fluence within brain tissue than for Top-hat beam.

Table 4. Mean numbers of light penetrated voxels within brain tissue. Std $< 0.01\%$Mean.

	$d = 2\,\mathrm{cm}$		$d = 4\,\mathrm{cm}$		$d = 6\,\mathrm{cm}$	
Beam diameter	Gaussian	Top-hat	Gaussian	Top-hat	Gaussian	Top-hat
Gray matter	1786,179	1798,549	1866,673	1878,757	1885,314	1898,444
White matter	670,060	670,643	698,219	704,139	699,450	701,834

Table 5. Accumulated fluence of light-penetrated voxels within brain tissue. Std $< 0.01\%$Mean.

	$d = 2$ cm		$d = 4$ cm		$d = 6$ cm	
Beam diameter	Gaussian	Top-hat	Gaussian	Top-hat	Gaussian	Top-hat
Gray matter	5.85e-2	1.18e-1	7.56e-2	7.93e-2	8.85e-2	8.33e-2
White matter	1.59e-3	1.26e-3	2.08e-3	2.17e-3	2.71e-3	2.38e-3

4. Conclusion and Discussion

This paper attempted to quantitatively study the effects of wavelength, beam size and beam type on LLLT dosage distribution in human head. We did not follow the previous widely used approach based on animal experiments or simplified tissue (e.g., layered tissue)-based dosage calculation. In this study, we proposed to address the optimization issue on LLLT illumination parameters by calculating and comparing light fluence (dosage) distributions in complex-structure-considered human head. In order to achieve high precision in fluence calculation, we combined the 3D Monte Carlo simulation software targeted for voxelized biological tissue (MCVM) and the most faithfully depicted Visible Human (VCH) model. We finally obtained the fluence distribution respective to LLLT treatments' commonly used wavelengths (660, 810 and 980 nm), beam diameters (2, 4 and 6 cm) and beam types (Gaussian and Top-hat beams). We visualized the data to intuitively compare the LLLT dosage respective to the variation of those illumination parameters. By comparison between Figs. 2 and 3, we can conclude that the wavelength ranked as the No. 1 effect on the LLLT fluence distribution, then beam size ranked as No. 2 and beam type ranked as No. 3. This finding was also verified by quantitative statics, which showed that wavelength affected in around $\sim 0-30$X range, beam size affected in $0-5$ 1% range, and beam type affected in $0-20\%$ range.

810 nm was shown to be the most proper wavelength, firstly since its penetration depth was the highest (around 0.5 cm deeper than 660 nm, 2 cm deeper than 980 nm), which agreed well with the experimental reports.[13,29] Additional quantitative evidences for preference of 810 nm included that the voxel numbers and accumulated fluence of light penetrated brain tissue for 810 nm were <1X higher than 660 nm and >3.5X higher than 980 nm.

Beam size increment can reduce the effect of the complex cerebral cortex folding geometry on fluence distribution and widen the $> 10^{-4}$ W/cm^2 fluence distribution. Statistics on light penetration within tissue acted <1X increment by beam size increment. The penetrated voxels within brain tissue for $d = 4$ cm and $d = 6$ cm beams were around 4.5% and 5.5% more than for $d = 2$ cm, respectively. The sum fluences within brain tissue for $d = 4$ cm and for $d = 6$ cm were 29% and 51% more than for $d = 2$ cm.

The Gaussian beam formed was more focused at $> 10^{-4}$ W/cm^2 fluence distribution than Top-hat beam, while statistics on light penetration within tissue showed that Top-hat beam has a stronger penetration than Gaussian beam in most cases. Firstly, Top-hat beam acted $<3\%$ stronger penetration than Gaussian beam for all diameter/wavelength setups by light penetrated brain tissue voxels. Secondly, Gaussian beam showed $<20\%$ higher accumulated fluence within brain tissue than that for Top-hat beam.

Our findings are helpful for researchers and clinicians in performing LLLT treatment on brain damage or diseases. As long as we get adequate simulations on full range for the illumination parameters, the data will be a potential to form a quantitative standard in guiding the optimized choosing illumination parameters for LLLT treatment, which would undoubtedly improve the LLLT treatment outcome.

Acknowledgments

This study was supported by the Research Start Fund (Grant No. Y02002010), the Central University Basic Scientific Research Project Business Expenses (Grant No. ZYGX2012J114) and the National Natural Science Foundation of China (Grant No. 61308114). We highly appreciate the Britton Chance Center for Biomedical Photonics in providing VCH dataset in this study.

References

1. S. R. Finfer, J. Cohen, "Severe traumatic brain injury," *Resuscitation* **48**, 77–90 (2001).
2. J. Nortje, D. K. Menon, "Traumatic brain injury: Physiology, mechanisms, and outcome," *Current Opin. Neurology* **17**, 711 (2004).
3. M. R. Hamblin, T. N. Demidova, "Mechanisms of low level light therapy," *Biomedical Optics*, pp. 614001–614012, International Society for Optics and Photonics (2006).
4. M. Bullock, J. Povlishock, "Guidelines for the management of severe traumatic brain injury. Editor's Commentary," *J. Neurotrauma* **24**, 1–2 (2007).
5. O. Demir, S. Singh, L. Klimaschewski, I. A. Kurnaz, "From birth till death: Neurogenesis, cell cycle, and neurodegeneration," *Anat. Rec.* **292**, 1953–1961 (2009).
6. Y. Y. Huang, M. Hamblin, L. Taboada, "Low-level laser therapy in stroke and central nervous system," *Handbook of Photonics for Biomedical Science*, Vol. 1, V. Tuchin, Ed., Series: Series in Medical Physics and Biomedical Engineering, pp. 717–737, CRC Press (2010).
7. N. Lane, "Cell biology: Power games," *Nature* **443**, 901–903 (2006).
8. Y. Y. Huang, A. Chen, M. Hamblin, "Advances in low-intensity laser and phototherapy," *Handbook of Photonics for Biomedical Science*, Vol. 1, V. Tuchin, Ed., Series: Series in Medical Physics and Biomedical Engineering, pp. 687–716, CRC Press (2010).
9. J. Tafur, E. P. A. V. Wijk, R. V. Wijk, P. J. Mills, "Biophoton detection and low-intensity light therapy: A potential clinical partnership," *Photomed. Laser Surg.* **28**, 23–30 (2010).
10. S. M. Rodrigo, A. Cunha, D. H. Pozza, D. S. Blaya, J. F. Moraes, J. B. B. Weber, M. G. de Oliveira, "Analysis of the systemic effect of red and infrared laser therapy on wound repair," *Photomed. Laser Surg.* **27**, 929–935 (2009).
11. J. Streeter, "Progress in low-level laser therapy," *Lasers and Electro-Optics Society, 2006, LEOS 2006, 19th Annual Meeting of the IEEE*, pp. 665–666, IEEE (2006).
12. T. Li, Q. Luo, S. L. Jacques, "Effect of cerebral cortex sulci on near-infrared light propagation during monitoring and treatment," p. BW4B.6, Optical Society of America, Biomed Opt. Annual Conf. (2012).
13. P. A. Lapchak, "Taking a light approach to treating acute ischemic stroke patients: Transcranial near-infrared laser therapy translational science," *Ann. Med.* **42**, 576–586 (2010).
14. L. Wang, S. L. Jacques, L. Zheng, "MCML–Monte Carlo modeling of light transport in multi-layered tissues," *Comput. Methods Programs Biomed.* **47**, 131–146 (1995).
15. T. Li, Q. Luo, H. Gong, "MCVM: Monte Carlo modeling of photon migration in voxelized media," *J. Innov. Opt. Health Sci.* **3**, 91–102 (2010).
16. G. Z. Zhang, Q. Liu, S. Q. Zeng, Q. M. Luo, "Organ dose calculations by Monte Carlo modeling of the updated VCH adult male phantom against idealized external proton exposure," *Phys. Med. Biol.* **53**, 3697–3722 (2008).
17. S. X. Zhang, P. A. Heng, Z. J. Liu, L. W. Tan, M. G. Qiu, Q. Y. Li, R. X. Liao, K. Li, G. Y. Cui, Y. L. Guo, X. P. Yang, G. J. Liu, J. L. Shan, J. J. Liu, W. G. Zhang, X. H. Chen, J. H. Chen, J. Wang, W. Chen, M. Lu, J. You, X. L. Pang, H. Xiao, Y. M. Xie, J. C. Cheng, "The Chinese Visible Human (CVH) datasets incorporate technical and imaging advances on earlier digital humans," *J. Anat.* **204**, 165–173 (2004).
18. P. A. Heng, S. X. Zhang, Y. M. Xie, T. T. Wong, Y. P. Chui, C. Y. Cheng, "Photorealistic virtual anatomy based on Chinese Visible Human data," *Clin. Anat.* **19**, 232–239 (2006).
19. G. Z. Zhang, Q. Liu, Q. M. Luo, "Monte Carlo simulations for external neutron dosimetry based on the visible Chinese human phantom," *Phys. Med. Biol.* **52**, 7367–7383 (2007).
20. G. Zhang, Q. Luo, S. Zeng, Q. Liu, "The development and application of the visible Chinese human model for Monte Carlo dose calculations," *Health Phys.* **94**, 118–125 (2008).
21. Q. Wu, Y.-Y. Huang, S. Dhital, S. K. Sharma, A. C.-H. Chen, M. J. Whalen, M. R. Hamblin, "Low level laser therapy for traumatic brain injury," *Proc. SPIE*, 755206-8 (2010).
22. P. A. Lapchak, L. De Taboada, "Transcranial near infrared laser treatment (NILT) increases cortical adenosine-5′-triphosphate (ATP) content following embolic strokes in rabbits," *Brain Res.* **1306**, 100–105 (2010).
23. M. A. Naeser, A. Saltmarche, M. H. Krengel, M. R. Hamblin, J. A. Knight, "Transcranial LED therapy for cognitive dysfunction in chronic, mild traumatic brain injury: Two case reports," *BiOS*, pp. 77512–77520, International Society for Optics and Photonics (2010).
24. T. Li, H. Gong, Q. Luo, "Visualization of light propagation in visible Chinese human head for functional near-infrared spectroscopy," *J. Biomed. Opt.* **16**, 045001 (2011).
25. A. Yaroslavsky, P. Schulze, I. Yaroslavsky, R. Schober, F. Ulrich, H. Schwarzmaier, "Optical properties of selected native and coagulated human brain tissues *in vitro* in the visible and near infrared spectral range," *Phys. Med. Biol.* **47**, 2059 (2002).

26. W. F. Cheong, S. A. Prahl, A. J. Welch, "A review of the optical properties of biological tissues," *IEEE J. Quantum Electron.* **26**, 2166–2185 (1990).
27. G. M. Hale, M. R. Querry, "Optical constants of water in the 200-nm to 200-μm wavelength region," *Appl. Opt.* **12**, 555–563 (1973).
28. C. R. Simpson, M. Kohl, M. Essenpreis, M. Cope, "Near-infrared optical properties of *ex vivo* human skin and subcutaneous tissues measured using the Monte Carlo inversion technique," *Phys. Med. Biol.* **43**, 2465 (1999).
29. P. Lapchak, K. Salgado, C. Chao, J. Zivin, "Transcranial near-infrared light therapy improves motor function following embolic strokes in rabbits: An extended therapeutic window study using continuous and pulse frequency delivery modes," *Neuroscience* **148**, 907–914 (2007).
30. T. Li, Y. Lin, Y. Shang, L. He, C. Huang, M. Szabunio, G. Yu, "Simultaneous measurement of deep tissue blood flow and oxygenation using noncontact diffuse correlation spectroscopy flow-oximeter," *Sci. Rep.* **3**, 1358 (2013).